Supplementary Materials: Modulating the Slow Relaxation Dynamics of Binuclear Dysprosium(III) Complexes through Coordination Geometry

Amit Kumar Mondal, Vijay Singh Parmar and Sanjit Konar

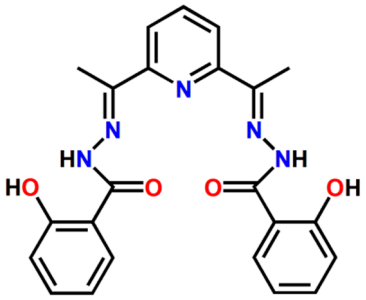

Figure S1. Structure of the pentadentate organic ligand L (L = 2,6-bis(1-salicyloylhydrazonoethyl) pyridine).

Table S1. Bond distances (Å) around Dy^{III} centers found in **1** and **2**.

Complex 1		Complex 2	
Dy1–O6	2.4382(6)	Dy1–O4	2.4364(1)
Dy1–O3	2.3855(5)	Dy1–O7	2.4771(1)
Dy1–O5	2.5639(4)	Dy1–O6	2.3976(1)
Dy1–O4	2.3103(5)	Dy1–O2	2.3553(1)
Dy1–O9	2.4086(5)	Dy1–N7	2.5471(1)
Dy1–N1	2.5268(5)	Dy1–N9	2.636(2)
Dy1–N3	2.5164(6)	Dy1–N6	2.7127(1)
Dy1–N4	2.4746(5)	Dy1–N1	2.6781(1)
Dy1–O1	2.3202(6)	Dy1–N2	2.5527(1)
		Dy1–N4	2.5479(1)
		Dy2–O9	2.3478(1)
		Dy2–O8	2.2724(1)
		Dy2–O10	2.2826(1)
		Dy2–N11	2.5059(1)
		Dy2–N12	2.4713(1)
		Dy2–O13	2.4213(1)
		Dy2–N14	2.4701(1)
		Dy2–O16	2.4171(1)

Table S2. Bond angles (°) around Dy^{III} centers found in **1** and **2**.

Complex 1		Complex 2	
O3–Dy1–O5	124.32(11)	O4–Dy1–O7	114.1(3)
O3–Dy1–O4	94.65(10)	O4–Dy1–O6	85.08(3)
O3–Dy1–O9	76.67(10)	O4–Dy1–O2	128.91(3)
O3–Dy1–N1	64.31(9)	O4–Dy1–N7	85.16(3)
O3–Dy1–N3	124.76(12)	O4–Dy1–N9	72.29(3)
O3–Dy1–N4	151.24(11)	O4–Dy1–N6	64.04(3)
O3–Dy1–O1	94.05(12)	O4–Dy1–N1	113.73(6)
O4–Dy1–O9	74.4(11)	O4–Dy1–N2	60.82(3)

Table S2. *Cont.*

Complex 1		Complex 2	
O4–Dy1–N1	146.13(13)	O4–Dy1–N4	161.11(4)
O4–Dy1–N3	125.07(14)	O7–Dy1–O6	128.38(4)
O4–Dy1–N4	65(9)	O7–Dy1–O2	81.99(3)
O4–Dy1–O1	139.77(15)	O7–Dy1–N7	157.37(4)
O5–Dy1–O4	71.58(9)	O7–Dy1–N9	61.32(3)
O5–Dy1–O9	140.96(13)	O7–Dy1–N6	116.51(3)
O5–Dy1–N1	141.97(11)	O7–Dy1–N1	65.63(3)
O5–Dy1–N3	105.38(12)	O7–Dy1–N2	68.75(3)
O5–Dy1–N4	70.45(9)	O7–Dy1–N4	80.66(3)
O5–Dy1–O1	71.12(8)	O6–Dy1–O2	123.81(4)
O6–Dy1–O3	73.18(10)	O6–Dy1–N7	62(3)
O6–Dy1–O5	51.16(9)	O6–Dy1–N9	157.03(4)
O6–Dy1–O4	74.2(11)	O6–Dy1–N6	114.96(3)
O6–Dy1–O9	133.9(14)	O6–Dy1–N1	62.8(3)
O6–Dy1–N1	119.52(12)	O6–Dy1–N2	83.15(3)
O6–Dy1–N3	146.86(14)	O6–Dy1–N4	76.27(3)
O6–Dy1–N4	116.54(12)	O2–Dy1–N7	76.38(3)
O6–Dy1–O1	70.99(12)	O2–Dy1–N9	75.53(3)
O9–Dy1–N1	74.98(10)	O2–Dy1–N6	65.48(3)
O9–Dy1–N3	79.24(11)	O2–Dy1–N1	116.94(4)
O9–Dy1–N4	78.24(10)	O2–Dy1–N2	149.39(4)
O9–Dy1–O1	145.72(16)	O2–Dy1–N4	62.39(3)
N1–Dy1–N3	61.69(9)	N7–Dy1–N9	118.2(3)
N1–Dy1–N4	121.61(10)	N7–Dy1–N6	59.77(3)
N1–Dy1–O1	71.33(10)	N7–Dy1–N1	119.01(3)
N3–Dy1–N4	62.9(9)	N7–Dy1–N2	133.61(4)
N3–Dy1–O1	79.5(12)	N7–Dy1–N4	83.46(3)
N4–Dy1–O1	114.65(12)	N9–Dy1–N6	58.57(3)
		O9–Dy2–O8	122.69(4)
		O9–Dy2–O10	96.82(4)
		O9–Dy2–N11	125.07(4)
		O9–Dy2–N12	64.28(3)
		O9–Dy2–O13	73.48(3)
		O9–Dy2–N14	151.62(4)
		O9–Dy2–O16	76.99(3)
		O8–Dy2–O10	112.29(4)
		O8–Dy2–N11	73.44(3)
		O8–Dy2–N12	89.87(3)
		O8–Dy2–O13	67.6(3)
		O8–Dy2–N14	85.34(3)
		O8–Dy2–O16	151.38(4)
		O10–Dy2–N11	127.18(4)
		O10–Dy2–N12	156.93(4)
		O10–Dy2–O13	76.37(3)
		O10–Dy2–N14	65.09(3)
		O10–Dy2–O16	82.56(4)
		N11–Dy2–N12	63.74(3)
		N11–Dy2–O13	140.33(3)
		N11–Dy2–N14	63.16(3)

Shape Analysis

Table S3. Summary of SHAPE analysis for complexes **1** and **2**.

Nine coordinate system: Complex **1**

EP-9 1 D_{9h} Enneagon
OPY-9 2 C_{8v} Octagonal pyramid
HBPY-9 3 D_{7h} Heptagonal bipyramid
JTC-9 4 C_{3v} Johnson triangular cupola J3
JCCU-9 5 C_{4v} Capped cube J8
CCU-9 6 C_{4v} Spherical-relaxed capped cube
JCSAPR-9 7 C_{4v} Capped square antiprism J10
CSAPR-9 8 C_{4v} Spherical capped square antiprism
JTCTPR-9 9 D_{3h} Tricapped trigonal prism J51
TCTPR-9 10 D_{3h} Spherical tricapped trigonal prism
JTDIC-9 11 C_{3v} Tridiminished icosahedron J63
HH-9 12 C_{2v} Hula-hoop
MFF-9 13 C_s Muffin

Complex 1. Nine coordinate Dy^{III} center.

[ML9]	EP-9	OPY-9	HBPY-9	JTC-9	JCCU-9	CCU-9	JCSAPR-9	CSAPR-9	JTCTPR-9	TCTPR-9	JTDIC-9	HH-9	**MFF-9**
Dy1	29.633	21.725	18.224	13.740	7.593	6.427	4.080	3.063	3.910	3.964	11.706	6.204	**2.565**

Eight coordinate system: Complex **2**

OP-8 1 D_{8h} Octagon
HPY-8 2 C_{7v} Heptagonal pyramid
HBPY-8 3 D_{6h} Hexagonal bipyramid
CU-8 4 O_h Cube
SAPR-8 5 D_{4d} Square antiprism
TDD-8 6 D_{2d} Triangular dodecahedron
JGBF-8 7 D_{2d} Johnson gyrobifastigium J26
JETBPY-8 8 D_{3h} Johnson elongated triangular bipyramid J14
JBTPR-8 9 C_{2v} Biaugmented trigonal prism J50
BTPR-8 10 C_{2v} Biaugmented trigonal prism
JSD-8 11 D_{2d} Snub diphenoid J84
TT-8 12 T_d Triakis tetrahedron
ETBPY-8 13 D_{3h} Elongated trigonal bipyramid

Complex 2. Eight coordinate Dy^{III} center.

[ML8]	OP-8	HPY-8	HBPY-8	CU-8	SAPR-8	**TDD-8**	JGBF-8	JETBPY-8	JBTPR-8	BTPR-8	JSD-8	TT-8	ETBPY-8
Dy1	34.479	22.854	9.299	8.632	5.331	**3.548**	8.211	26.049	4.388	3.584	6.084	9.351	22.822

Ten coordinate system: Complex **2**

DP-10	1	D_{10h}	Decagon
EPY-10	2	C_{9v}	Enneagonal pyramid
OBPY-10	3	D_{8h}	Octagonal bipyramid
PPR-10	4	D_{5h}	Pentagonal prism
PAPR-10	5	D_{5d}	Pentagonal antiprism
JBCCU-10	6	D_{4h}	Bicapped cube J15
JBCSAPR-10	7	D_{4d}	Bicapped square antiprism J17
JMBIC-10	8	C_{2v}	Metabidiminished icosahedron J62
JATDI-10	9	C_{3v}	Augmented tridiminished icosahedron J64
JSPC-10	10	C_{2v}	Sphenocorona J87
SDD-10	11	D_2	Staggered Dodecahedron (2:6:2)
TD-10	12	C_{2v}	Tetradecahedron (2:6:2)
HD-10	13	D_{4h}	Hexadecahedron (2:6:2) or (1:4:4:1)

Complex 2. Ten coordinate Dy^{III} center.

[ML_{10}]	DP-10	EPY-10	OBPY-10	PPR-10	PAPR-10	JBCCU-10	**JBCSAPR-10**	JMBIC-10	JATDI-10	JSPC-10	SDD-10	TD-10	HD-10
Dy2	32.605	23.770	16.774	10.267	8.604	5.452	**3.125**	6.212	17.465	3.736	4.292	3.882	3.760

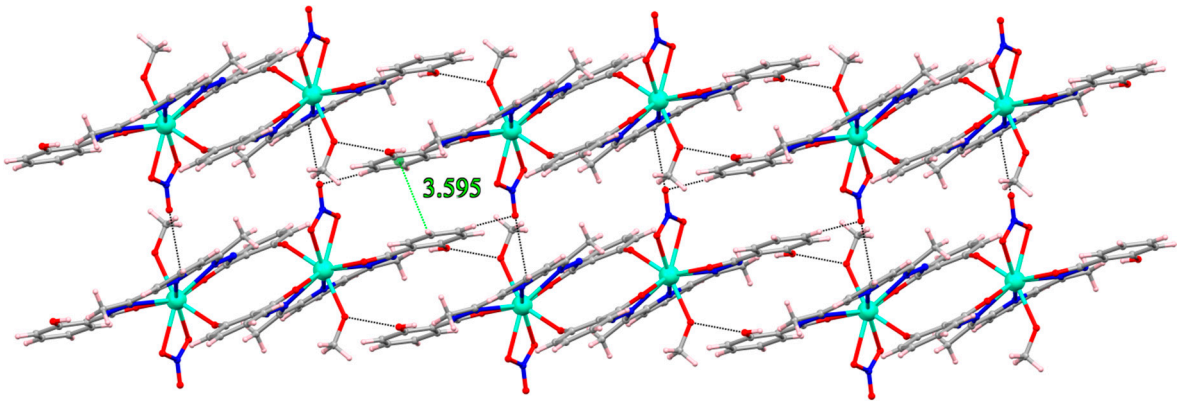

Figure S2. A view of supramolecular 2D arrangement of complex **1** through intermolecular H-bonding and CH···π interactions.

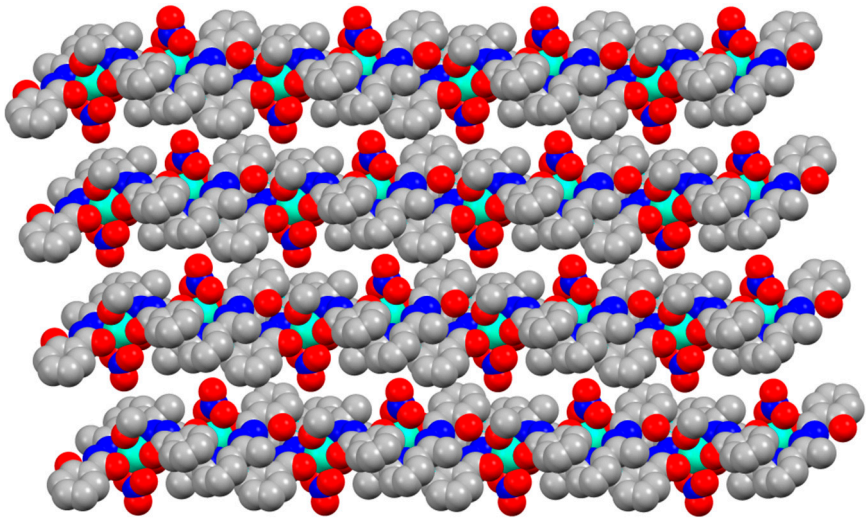

Figure S3. A view of de-solvated framework of **1** emphasizing the supramolecular interactions.

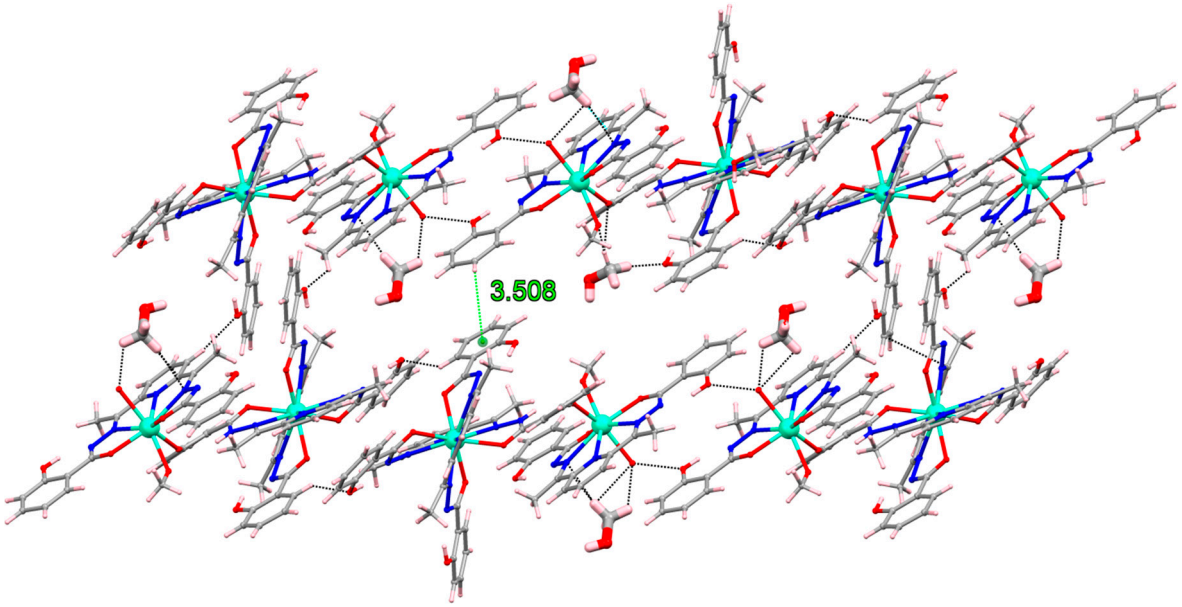

Figure S4. A view of supramolecular 2D arrangement of complex **2** through intermolecular H-bonding and CH···π interactions.

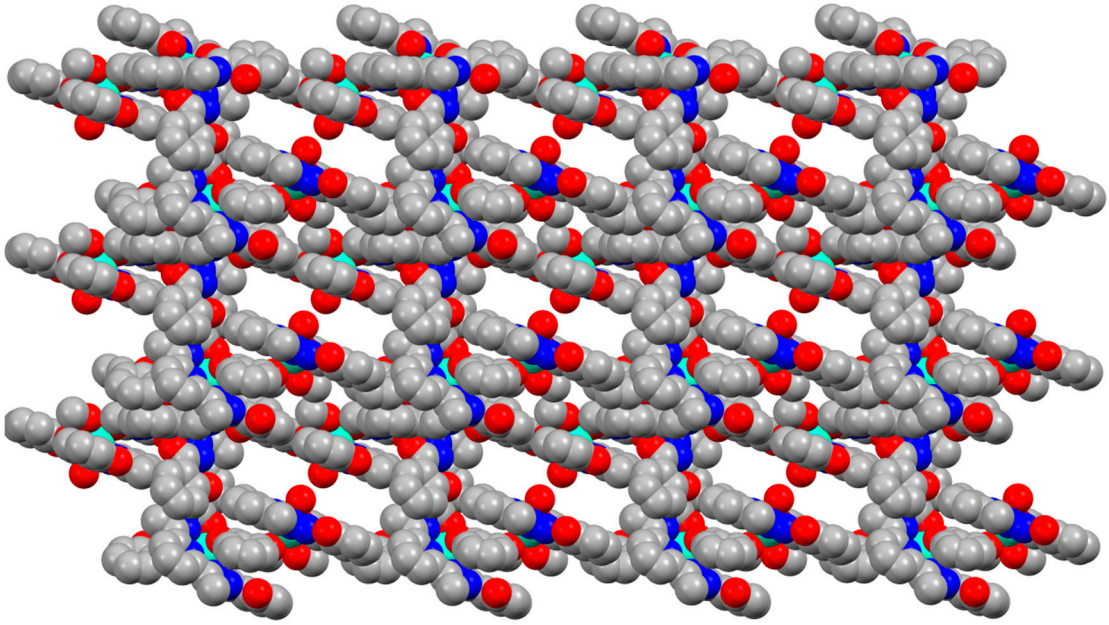

Figure S5. A view of de-solvated framework of **2** emphasizing the supramolecular interactions.

Table S4. H-bond parameters found in complex **1**.

D–H···A	D–H(Å)	H···A(Å)	D···A(Å)	<D-H-A(°)	Symmetry [#]
O(2)–H(2)..N(5)	0.82	1.80	2.521(6)	147	0
C(17)–H(17)..O(4)	0.93	2.48	2.791(8)	100	0
C(22)–H(22C)..N(5)	0.96	2.39	2.808(8)	106	0
C(23)–H(23A)..N(2)	0.96	2.42	2.827(8)	105	0
C(19)–H(19)..O(7)	0.93	2.50	3.432(9)	176	1
C(27)–H(27A)..O(4)	0.97	2.30	3.250(11)	167	2

[#] (0) *x*, *y*, *z*; (1) 1 + *x*, −1 + *y*, 1 + *z*; (2) *x*, 1 + *y*, *z*.

Table S5. H-bond parameters found in complex **2.**

D–H···A	D–H(Å)	H···A(Å)	D···A(Å)	<D-H-A(°)	Symmetry #
O11A–H11A..O9	0.84	2.18	2.9727(2)	147	0
C025–H02C..O5	0.98	2.12	2.9015(2)	136	1
C74–H74C..O11A	0.98	1.53	2.5086(2)	175	1
C62–H62B..O1	0.98	2.57	3.2954(2)	130	2
C72–H72B..O13	0.98	1.74	2.6951(2)	165	3
C72–H72C..O3	0.98	1.88	2.7867(2)	153	3
C74–H74A..N12	0.98	2.41	3.3478(2)	160	4
C74–H74B..O16	0.98	2.28	2.8858(2)	119	4

(0) *x*, *y*, *z*; (1) 1 − *x*, 1 − *y*, 1 − *z*; (2) 1 − *x*, −*y*, 1 − *z*; (3) 1 + *x*, *y*, *z*; (4) *x*, 1 + *y*, *z*.

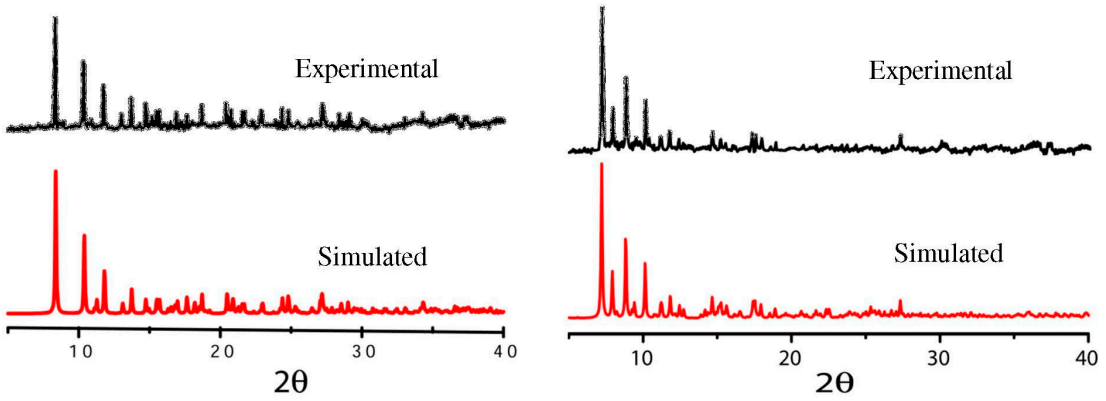

Figure S6. PXRD patterns of complex **1** (**left**) and **2** (**right**).

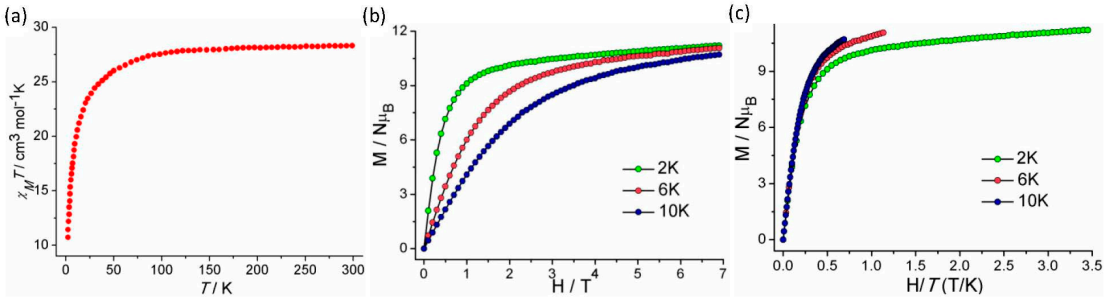

Figure S7. (**a**) $\chi_M T$ vs. *T* plot measured at 0.1 T for complex **2**; *M*/*N*μB vs. H (**b**) and *M*/*N*μB vs. H/*T* plots (**c**) in the field range of 0–7 T and temperature range of 2–10 K for complex **2.**

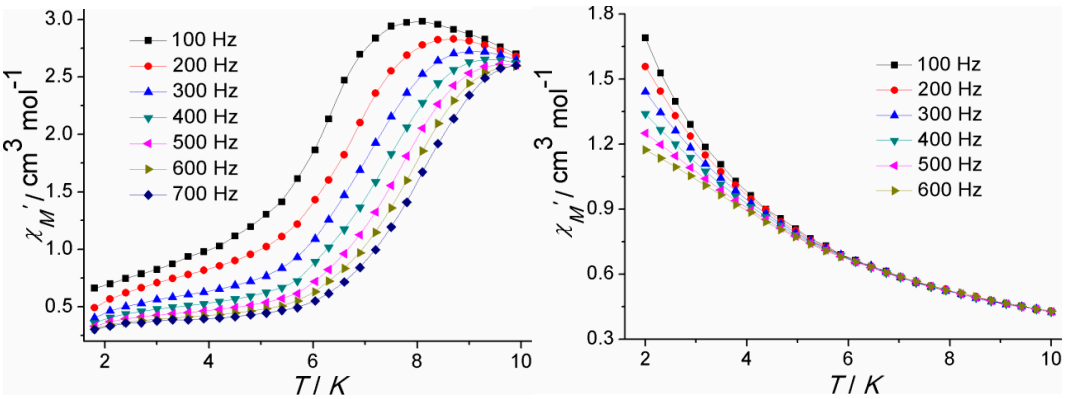

Figure S8. Temperature dependency of the in-phase (χ_M') AC magnetic susceptibility plots for complexes **1** (**left**) and **2** (**right**) under 0 Oe dc field.

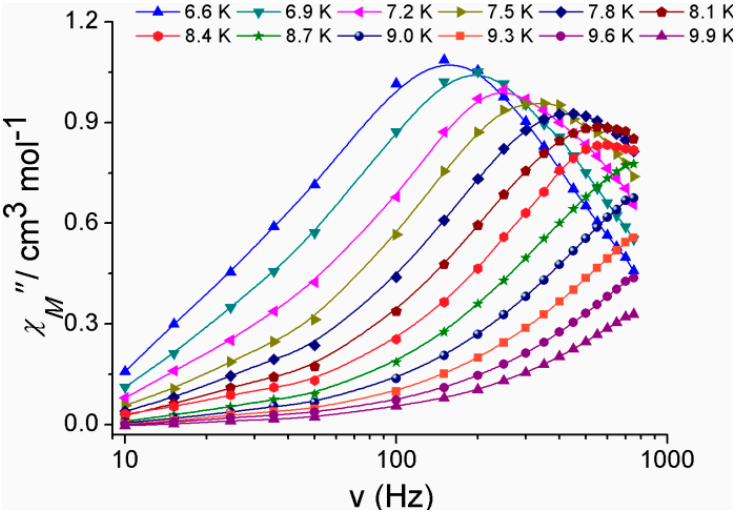

Figure S9. Frequency dependency of the out-of phase ac susceptibility plots for complex **1** under 0 Oe dc field.

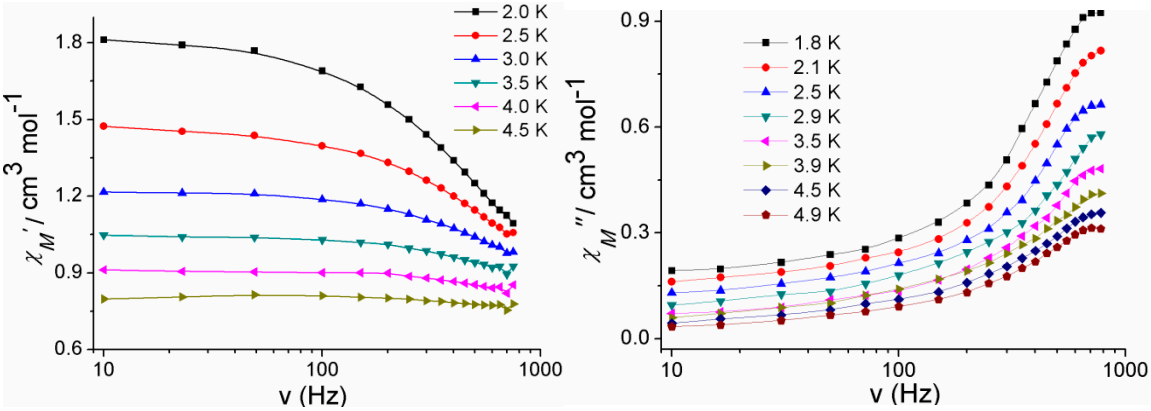

Figure S10. Frequency dependency of the in-phase (**left**) and out-of phase (**right**) ac susceptibility plots for complex **2** under 0 Oe dc field.

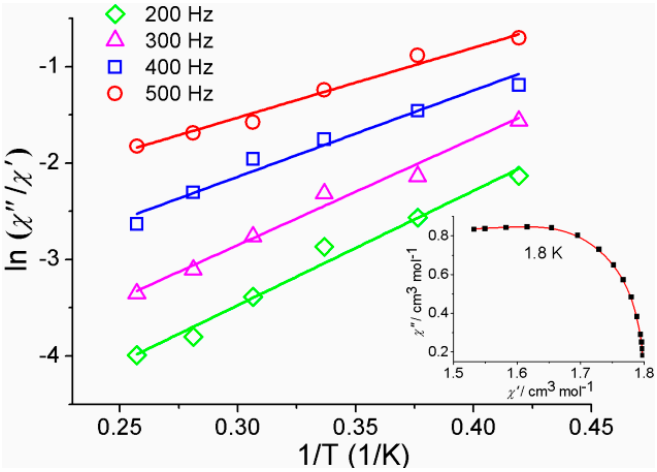

Figure S11. Natural logarithm of the ratio of χ_M'' over χ_M' vs. $1/T$ for **2** (solid lines represent best fit obtained from Equation (2). Cole-Cole plots for **2** are shown in the inset.

Experimental Information for Dilution Studies:

Synthesis of $[Y_2(L)_2(MeOH)_2(NO_3)_2]\cdot(MeOH)$ (MeCN) (3)

L (43 mg, 0.1 mmol) was dissolved in MeCN (5 mL) and the solution was warmed to 45 °C. Deprotonation of ligand was performed by $LiOH\cdot H_2O$ (4.0 mg, 0.1 mmol). Then, $Y(NO_3)_3\cdot 6H_2O$ (39 mg, 0.1 mmol) dissolved in MeOH (5 mL) was added to the above ligand solution while stirring. The solution formed an intense yellow mixture that was stirred for another 2 h. The solution was then filtered off and the filtrate was left in open atmosphere for slow evaporation which gives large X-ray quality yellow crystals of $[Y_2(L)_2(MeOH)_2(NO_3)_2]\cdot(MeOH)$ (MeCN) (**3**) after 4 days. The crystals were separated and washed with cold water and Et_2O; yield (60%). Anal. Calcd for $C_{51}H_{51}Y_2N_{13}O_{17}$: C, 47.28; H, 3.97; N, 14.05%. Found: C, 47.39; H, 4.04; N, 14.13%. Selected IR data (KBr pellet, 4000–400 cm^{-1}) ν/cm^{-1}: 3420 (s), 2914 (w), 1767 (w), 1603 (s), 1569 (s), 520 (w).

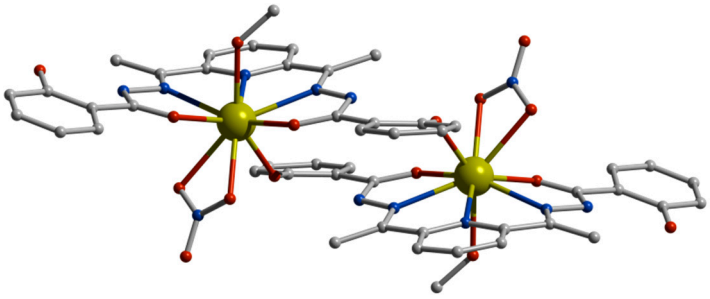

Figure 12. View of the molecular structure of complex **3**.

Table S6. X-ray Crystallographic Data and Refinement Parameters for **3**.

	3
Formula	$C_{54}H_{58}Y_2N_{14}O_{18}$
M_w ($g\cdot mol^{-1}$)	1368.96
Crystal size (mm)	0.42 × 0.14 × 0.13
Crystal system	Triclinic
Space group	*P*-1
T (K)	106(2)
a (Å)	10.7427(15)
b (Å)	10.7992(16)
c (Å)	12.829(3)
α (°)	84.608(12)
β (°)	85.633(8)
γ (°)	78.155(7)
V ($Å^3$)	1447.7(5)
Z	1
ϱ_{calcd} ($g\cdot cm^{-3}$)	1.570
μ(MoKα) (mm^{-1})	2.080
F(000)	702.0
T_{max}, T_{min}	0.753, 0.722
h, *k*, *l* range	$-14 \le h \le 14$, $-14 \le k \le 14$, $-17 \le l \le 17$
Collected reflections	7789
Independent reflections	4209
Goodness-of-fit (GOF) on F^2	1.079
*R*1, *wR*2 ($I > 2\sigma I$)	0.0759, 0.1663
*R*1, w*R*2 (all data)	0.1328, 0.1940
CCDC Number	1482443

$R1 = \Sigma||Fo| - |Fc||/\Sigma|Fo|$ and $wR2 = |\Sigma w(|Fo|^2 - |Fc|^2)|/\Sigma|w(Fo)^2|^{1/2}$.

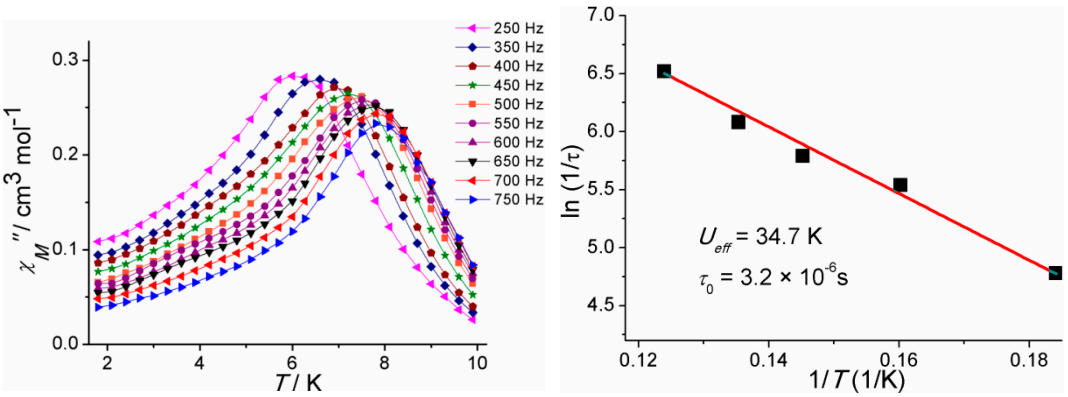

Figure S13. Out-of-phase (χ_M'') ac magnetic susceptibility plot for diluted sample at 0 Oe dc field (**left**). Illustration of ln(1/τ) vs. 1/*T* plots (**right**) for diluted sample (red lines represents the best fit of the Arrhenius relationship).